Section A-Research paper

Study of Multiple Slip effects on flow of nanofluid a three-dimensional direction of Stretching Sheet in the presence of Magnetic field using Finite Element Method

K. G. R. Deepthi*, S. Kavitha[1] and V. Vasudeva Murthy[2]

*Research Scholar, Annamalai University, Annamalai Nagar, Chidambaram

** Department of Mathematics, Vishnu Institute of Technology, Bhimavaram, West Godavari, 534302, Andhra Pradesh, India.*

[1] Department of Mathematics, Annamalai University, Annamalai Nagar, 608002, Tamilnadu State, India.

[2]Department of Mathematics, S. R. K. R. Engineering College, Bhimavaram, West Godavari, 534201,Andhra Pradesh, India.

**Corresponding author Email address: deepthi.k@vishnu.edu.in*

Abstract: This article analyses the numerical flow of three-dimensional of an electrically conducting, incompressible, and slip has been used to study viscous nanofluid flow, motion of Brownian, and effects of thermophoresis. This study was executed in the presence of Brownian motion ,slip and thermophoresis effects. When a magnetic field is produced, a surface that can be stretched and is permeable that also induces flow can conduct electricity. Through the use of the essential modifications, system of partial differentials that is not linear may be turned into system of an ordinary differential. After completing any necessary transformations of self-similarity, the governing equations are next subjected to a numerical solution with the assistance of the finite element method. Graphs are applied in the process of explaining the effect that the non-dimensional regulating factors have on velocity, temperature,and concentration profiles. Calculating and displaying the skin-friction coefficients, Sherwood number, and Nusselt number may all be done with the help of tables. The latest results, it is determined, display a significant deal of consistency with the conclusions of the earlier examinations, notwithstanding some unique situations.

Keywords: Slip effects; Three-dimensional; MHD; Nanofluid; Stretching sheet; Finite element method;

Nomenclature:

List of Symbols:

u, v, w **:** Velocity components (m/s) x, y, and z axes, respectively.

x, y, z **:** Measurements made using Cartesian coordinates along the stretched sheet (m)

f **:** Along x - direction Dimensionless stream function (kg / $m.\ s$)

f' **:** velocity of along x – axis (m/s)

g **:** Function along the direction of y Dimensionless stream (kg / $m.\ s$)

g' **:** Along y - direction Fluid velocity (m/s)

Pr**:** Prandtl number

T**:** Fluid Temperature (K)

T_w **:** **S**urface Temperature (K)

Eur. Chem. Bull. 2023, 12(Special Issue 4), 13142-13163

B_o **:** Uniform magnetic field (*Tesla*)

M **:** Magnetic field parameter

T_∞ **:** Fluid Temperature of the Stretching Sheet's Distant Fluid (*K*)

Cf **:** coefficient of Skin-friction along *x*-direction (s^{-1})

$u_w(x)$**:** Stretching of fluid velocity along *x*-direction (*m*/*s*)

$v_w(y)$**:** Stretching fluid velocity along *y* - direction(*m*/*s*)

Nu **:** Rate of Heat transfer coefficient (or) Nusselt number

Sh **:** Rate **of M**ass transfer coefficient (or) Sherwood number

C_p **:** Nano particles Specific heat capacity ($J / kg / K$)

a **:** Constant

Re_x **:** Reynolds number

C **:** Volume concentration Fluid nanoparticle (mol/m^3)

C_∞ **:** Volume fraction of Dimensional ambient (mol/m^3)

Nb **:** Parameter of Brownian motion

Nt **:** Parameter of Thermophoresis

A: Coefficient related to stretching sheet

Le **:** Lewis number parameter

p **:** Pressure (*pa*)

D_B: Coefficient of Brownian diffusion (m^2 / s)

C_w **:** Nanoparticle with dimensions volume concentration at the stretching surface (mol/m^3)

n: Velocity power index parameter

D_T : Coefficient of Thermophoresis diffusion (m^2 / s)

h_1^* : Parameter for slip in dimensional velocity

h_2^* : Temperature jump in the parameter dimension

h_3^* : Parameter Dimensional concentration jump

h_1 : Dimensionless velocity slip as a parameter

h_2 : Jump parameterDimensionless temperature

h_3 : Jump parameter for concentration without dimensions

b: Coefficient Thermal accommodation

d: Coefficient Concentration accommodation

f_1 : Maxwell's reflection coefficient

Greek symbols:

η **:** Dimensionless similarity variable (*m*)

θ **:** Dimensionless temperature (*K*)

ν **:** Kinematic viscosity (m^2 / s)

σ **:** Electrical Conductivity

μ **:** Fluid Dynamic viscosity

κ **:** Fluid Thermal conductivity

ρ_f **:** Fluid Density (kg / m^3)

τ **:** Effective heat capacitance

γ **:** Ratio of specific heats

ϕ: At the stretching surface Nanoparticle volume concentration (mol/m3)

λ: Wall thickness parameter

κ_B: Boltzmann constant (J/K)

ξ_1: Mean free path (constant)

ξ_2: Mean free path (constant)

ξ_3: Mean free path (constant)

Superscript:

$'$: Derivative w.r.t z

Subscripts:

f: Fluid

w: condition of the sheet

∞: Ambient circumstances

1. Introduction:

An electrically conductive fluid when a magnetic field is applied, MHD forces are produced as a result of electric currents being induced in one another and the applied magnetic field. In the great majority of manufacturing and production procedures, such as crystal, pumping, and metal casting formation, and the cooling of fission reactor circuits, magnetic fields are used. Uddin and Kumar [1] examined the flow of a micropolar fluid through a wedge and the effects of ion-slip and Hall depending on the boundary layer's thickness. Makinde and Mutuku-Njane [2] have examined the flow of a nanofluidic boundary layer with MHD across a Newtonian heating and pores on the surface. Their results are available in [2]. Recent study by Ablel-Rahman [3] examined the influence of MHD as well as the mass transfer flow over a porous substance. Abdelmeguid and Seddeek [4] evaluated explained the results of ion-slip currents and Hall currents' effects on the boundary layer studies on a horizontal plate's steady magneto-micropolar fluid. Additionally, they discussed the boundary layer's consequences. Ahmed and Batin [5] studied MHD movement via porous media by considering the magnetic field effects that is produced and viscous dissipation together. Ram [6] examined impacts of Hall and ion slip currents on MHD spinning free convective heat-generating flow. Jha and Apere [7] examined the unsteady MHD Newtonian fluid in the between two parallel spinning plates, a couette flow occurs.. They analysed the flow while accounting for ion-slip and hall currents. Sharma et al. [8] investigated the radiation effect on MHD flow when channelled via an accelerating vertical plate. Oztop and Abu-Nada [9] did research on the computational examination of naturally heated air through convection, nanofluid-filled rectangular enclosures. Reddy et al. examined in the presence of ohmic heating the effects of thermal and mass diffusion on MHD flow in their work [10]. Seddeek [11] examines the effects of Hall and ion-slip currents, as well as heat transfer and stretching with suction and blowing, on magneto-micropolar fluid across a non-isothermal sheet. In the setting he does this with suction, blowing, and a non-isothermal stretched sheet.. Sara and Bhatti [12] examined the unstable

magnetohydrodynamic (MHD) non-Newtonian nanofluid moving peristaltically containing chemical reaction, ion and Hall slip currents. In their work [13], Jitendra and Srinivas examined of Ion slip and Hall effects on an unstable a spinning fluid's crossing a vertical plate with natural convection moving at an increasingly faster pace. Ibanez [14] studied magnetohydrodynamic flow in a porous channel while taking into account the condition of a convective barrier. Formation of entropy was another subject of his studies. Aziz [15] identified the similarity solutions on a boundary condition on a flat plate for convective surfaces.

When nanofluid is added to a stretched sheet, a boundary layer flow happens. This is a major type of flow. This is because it is used in a lot of different fields, like polymer engineering and metallurgy. This course covers topics like the petrochemical industry, polymerization, polymer structure and characterization, polymer properties, polymer compounding and processing, and an overview of the most important polymers. Researchers have been putting a lot of time and effort into studying nanofluids lately because they have better thermal properties. Nanoparticles, which can be carbon nanotubes, oxides, carbides, or metals, are mixed in with the basic liquid to make these fluids. The nanoparticles can come in many different shapes and sizes. Ethylene glycol, water, and oil are all examples of basic fluids that people usually use. The main advantages of using nanofluids instead of the thermal conductivity of the base fluid is that, and coefficient of convective heat transfer both go up. Nanomaterials can transfer heat more efficiently, which makes them a good choice for meeting the growing needs of modern technology in places like power plants, the chemical industry, and microelectronics. In many applications Magneto-nanofluids are used, such as optical switches, tunable optical fibre filters, optical modulators, and magneto-optical wavelength filters. metallic nanoparticles can be used to treat cancer, sort things into those that sink and those that float, and in biomedicine. Nanofluids have many different uses in the field of biomedicine. For example, they can be used to treat hyperthermia, separate cells using magnets, deliver drugs, and improve contrast in MRIs. A lot of research has been done on the flow of nanofluids with many different kinds of properties. Khan et al. [16] looked at how a nanofluid flows continuously in three dimensions over a surface that is stretched in a way that is not linear. This was done when there is thermophoresis and Brownian motion and. Hayat et al. [17] looked at an unstable magneto-nanofluid that had two layers of stratification. They did this by stretching a sheet at an angle. Ferdows et al. [18] looked at how the nanofluid moved across the plate and how heat was made. Sravan Kumar et al. [19] used MHD to study and analyse the data that was collected after putting a water-based nanofluid with three distinct nanoparticles is flowing across a vertical panel that stimulated numbers. Reddy et al. [20] did an experiment to find out how radiation affects the nanofluid mass and heat transfer past a material-embedded vertical plate that absorbs radiation. Hussain et al. [21] did research that

looked at how radiation affected the MHD nanofluid as it moved through a medium that absorbed it. Anjali Devi and her colleagues [22] did research on how nanofluids move across an angled plate based on the Blasius and Sakiadis model. Lin et al. [23] made a model for heat transmission and MHD pseudo-plastic nanofluid flow instability in a finite thin sheet with internal heat production over a stretched surface. This model was used to study heat transmission and MHD pseudo-plastic nanofluid flow that is erratic in a finite thin sheet with internal heat production. When Farroq et al. [24] looked at the MHD stagnation point flow, they focused on a nanofluid that was viscoelastic and could cause non-linear radiation effects. Hayat et al. [25] looked at the two-dimensional Williamson nanofluid MHD flow with surface melting heat transfer that thickens and thins in a nonlinear way. Nadeem et al. [26] looked at how partial sliding affected the a nanofluid's stagnation point at the edge of a stretched surface under a boundary condition for convection. Hayat et al. looked at the impact of a convective boundary condition and a three-dimensional flow of a magnetic field across a surface that was not stretched in a straight line in their paper [27]. Lopez et al. [28] looked at the MHD nanofluid flow with increased entropy in a convective-radiative boundary-condition microchannel that is vertically porous. A vertical microchannel was used to do this work. Rajesh et al. [29] did research on the analytical a method of scaling the wall temperature and thermal radiation while conducting flow of MHD hybrid nanofluid over an infinite vertical plate. Siavashi and his researchers [30] on An annulus that is heated on both sides can transmit heat more efficiently by using forced convection in a porous material.. This is accomplished by placing nanoparticles within the base fluid and adding them there.

The objective of this article, which was motivated by the aforementioned research, is to examine the consequences of flow in an electrically conducting fluid with respect to velocity, temperature, and concentration slips, incompressible, steady, three-dimensional Thermophoresis and Brownian motion phenomena in nanofluid, and a magnetic field. The temperature ,velocity, and concentration slip conditions in a nanofluid flow may have an important effect on the rate of heat transfer and nanoparticles motion. Mathematical models of the flow phenomena are developed using the fundamental principles of motion. The Ordinary derivable equations are created from controlling partial derivable equations. via similarity transformations. The simplified differential equations that are linked together is ultimately resolved numerically the use of the finite element method. To determine the impacts of various physical characteristics, a thorough parametric analysis is conducted using graphs and numbers. When the data were compared to what had already been published, it became clear that they were remarkably similar.

2. Flow Governing Equations:

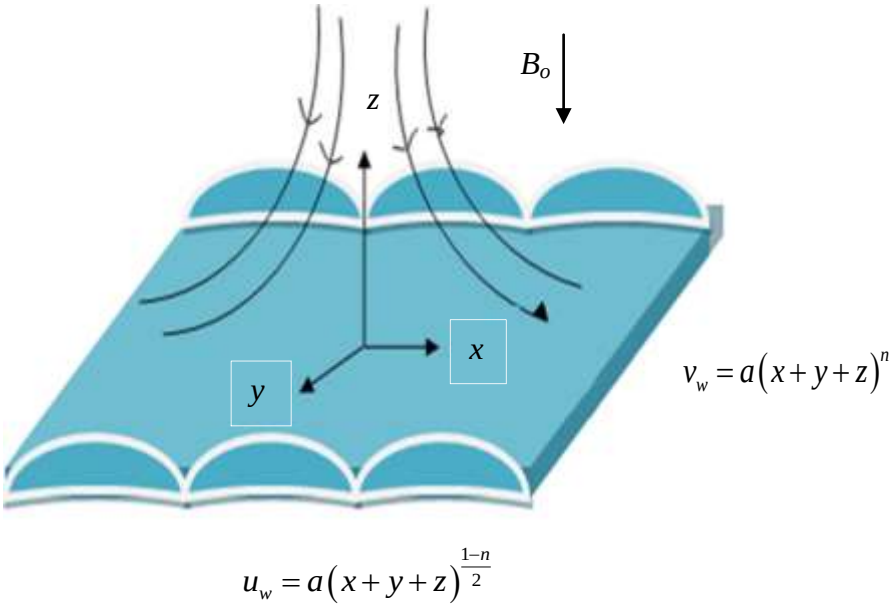

Fig. 1. Flow geometry

In this present research manuscript,electrically conductive fluid flowing in three dimensions,incompressible, viscous nanofluid flow toward a stretched sheet when thermophoresis is present., Brownian motion, slip and Magnetic field effects are studied. The flow of geometry is as demostrate in the Fig. 1. For this research, the following assumptions are made:

a) The stretched sheet's varying thickness might be characterised as $z = A(x+y+z)^{\frac{1-n}{2}}$.

b) It is also supposing that the stretched sheet's s velocity is $u_w = a(x+y+z)^{\frac{1-n}{2}}$ and this applies to $n \neq 1$ thus n - 1 relates to the situation for a flat sheet.

c) It is to disregard the magnetic field created, the magnetic Reynolds number was thought to be as low as feasible..

d) With in this work, the authors have decided to consider the of Brownian motion and thermophoresis impact of a powerful magnetic field B_o is used to the flow.

The governing equations as per the above assumptions, are given as follows

Continuity Equation:

$$\frac{\partial u}{\partial x} + \frac{\partial v}{\partial y} + \frac{\partial w}{\partial z} = 0 \qquad (1)$$

Momentum Equations:

$$u\left(\frac{\partial u}{\partial x}\right)+v\left(\frac{\partial u}{\partial y}\right)+w\left(\frac{\partial w}{\partial z}\right)=\nu\left(\frac{\partial^2 u}{\partial z^2}\right)-\left(\frac{\sigma B_o^2}{\rho_f}\right)u \tag{2}$$

$$u\left(\frac{\partial u}{\partial x}\right)+v\left(\frac{\partial u}{\partial y}\right)+w\left(\frac{\partial w}{\partial z}\right)=\nu\left(\frac{\partial^2 v}{\partial z^2}\right)-\left(\frac{\sigma B_o^2}{\rho_f}\right)v \tag{3}$$

Equation of thermal energy:

$$u\left(\frac{\partial T}{\partial x}\right)+v\left(\frac{\partial T}{\partial y}\right)+w\left(\frac{\partial T}{\partial z}\right)=\frac{\kappa}{\rho C_p}\left(\frac{\partial^2 T}{\partial z^2}\right)+\tau\left[D_B\frac{\partial T}{\partial z}\frac{\partial C}{\partial z}+\frac{D_T}{T_\infty}\left(\frac{\partial T}{\partial z}\right)^2\right] \tag{4}$$

Equation of species concentration:

$$u\left(\frac{\partial C}{\partial x}\right)+v\left(\frac{\partial C}{\partial y}\right)+w\left(\frac{\partial C}{\partial z}\right)=D_B\left(\frac{\partial^2 C}{\partial z^2}\right)+\frac{D_T}{T_\infty}\left(\frac{\partial^2 T}{\partial z^2}\right) \tag{5}$$

The boundary conditions for this flow are

$$\left.\begin{aligned} &u=u_w(x)+h_1^*\left(\frac{\partial u}{\partial z}\right),\ v=v_w(x)+h_1^*\left(\frac{\partial v}{\partial z}\right),\ T=T_w(x)+h_2^*\left(\frac{\partial T}{\partial z}\right),\quad C=C_w(x)+h_3^*\left(\frac{\partial C}{\partial z}\right)\ \ at\ \ z=0\\ &u\to 0,\ v\to 0,\ T\to T_\infty,\ C\to C_\infty\ \ as\ \ z\to\infty\end{aligned}\right\} \tag{6}$$

where

$$\left.\begin{aligned} h_1^*&=\left[\frac{2-f_1}{f_1}\right]\xi_1(x+y+z)^{\frac{1-n}{2}},\ \xi_1=\frac{\kappa_B T}{\sqrt{2}\pi d^2 p},\\ h_2^*&=\left[\frac{2-b}{b}\right]\xi_2(x+y+z)^{\frac{1-n}{2}},\ \xi_2=\left[\frac{2\gamma}{\gamma+1}\right]\frac{\xi_1}{\mathrm{Pr}},\\ h_3^*&=\left[\frac{2-d}{d}\right]\xi_3(x+y+z)^{\frac{1-n}{2}},\ \xi_3=\left[\frac{2\gamma}{\gamma+1}\right]\frac{\xi_2}{\mathrm{Pr}},\\ B(x)&=B_o(x+y+z)^{\frac{1-n}{2}},\end{aligned}\right\} \tag{7}$$

$$\left.\begin{aligned} u_w&=a(x+y+z)^{\frac{1-n}{2}},\\ v_w&=a(x+y+z)^n,\\ \tau&=\frac{(\rho C_p)_s}{(\rho C_p)_f},\\ T_w&=T_\infty+T_o(x+y+z)^{\frac{1-n}{2}},\\ C_w&=C_\infty+C_o(x+y+z)^{\frac{1-n}{2}},\end{aligned}\right\}\ \ for\ \ n\neq 1 \tag{8}$$

The authors converted the governing equations into ordinary differential equations and introduced the following similarity transformations.

$$\left.\begin{aligned} &u = a\left(x+y+z\right)^{n} f'\left(\eta\right),\ \theta = \frac{T-T_{\infty}}{T_{w}\left(x\right)-T_{\infty}},\ \phi = \frac{C-C_{\infty}}{C_{w}\left(x\right)-C_{\infty}},\\ &v = a\left(x+y+z\right)^{n} g'\left(\eta\right),\ \eta = z\left(\sqrt{\frac{\left(n+1\right)a}{2\nu}}\right)\left(x+y+z\right)^{\frac{1-n}{2}},\\ &w = -\sqrt{\frac{2a\nu}{n+1}}\left(x+y+z\right)^{\frac{1-n}{2}}\left\{\left(\frac{n+1}{2}\right)\left[f\left(\eta\right)+g\left(\eta\right)\right]+\eta\left(\frac{n-1}{2}\right)\left[f'\left(\eta\right)+g'\left(\eta\right)\right]\right\} \end{aligned}\right\} \tag{9}$$

Equation of continuity is identically satisfied and Eqs. (2), (3), (4) and (5) take the following form, making use of Eq. (9)

$$\left(\frac{n+1}{2}\right)f''' - nf'^{2} - nf'g' + \left(\frac{n+1}{2}\right)ff'' + \left(\frac{n+1}{2}\right)gf'' - Mf' = 0 \tag{10}$$

$$\left(\frac{n+1}{2}\right)g''' - ng'^{2} - nf'g' + \left(\frac{n+1}{2}\right)fg'' + \left(\frac{n+1}{2}\right)gg'' - Mg' = 0 \tag{11}$$

$$\theta'' + Nb\theta'\phi' + Nt\theta'^{2} - \left(\frac{1-n}{1+n}\right)\mathrm{Pr}\, f'\theta - \left(\frac{1-n}{1+n}\right)\mathrm{Pr}\, g'\theta + \left(\frac{1-n}{1+n}\right)\mathrm{Pr}\, f\theta' + \left(\frac{1-n}{1+n}\right)\mathrm{Pr}\, g\theta' = 0 \tag{12}$$

$$Nb\phi'' + Nt\theta'' + LeNb\left(\frac{1-n}{1+n}\right)f'\phi - NbLe\left(\frac{1-n}{1+n}\right)g'\phi + NbLe\left(\frac{1-n}{1+n}\right)f\phi' + NbLe\left(\frac{1-n}{1+n}\right)g\phi' = 0 \tag{13}$$

and the corresponding boundary conditions (6) becomes

$$\left.\begin{aligned} &f\left(0\right) = \lambda\left(\frac{1-n}{1+n}\right)\left[1+h_{1}f''\left(0\right)\right],\ g\left(0\right) = \lambda\left(\frac{1-n}{1+n}\right)\left[1+h_{1}g''\left(0\right)\right],\\ &f'\left(0\right) = 1+h_{1}f''\left(0\right),\ g'\left(0\right) = 1+h_{1}g''\left(0\right),\\ &\theta\left(0\right) = 1+h_{2}\theta'\left(0\right),\ \ \phi\left(0\right) = 1+h_{3}\phi'\left(0\right),\\ &f'\left(\infty\right) = 0,\ g'\left(\infty\right) = 0,\ \theta\left(\infty\right) = 0,\ \ \phi\left(\infty\right) = 0, \end{aligned}\right\} \tag{14}$$

here the involved physical parameters are defined as

$$\left.\begin{aligned} &M = \frac{\sigma B_{o}^{2}}{\rho a},\ \mathrm{Pr} = \frac{\mu C_{p}}{\kappa},\ \lambda = \sqrt{\frac{\left(n+1\right)a}{2\nu}},\ Le = \frac{\nu}{D_{B}},\ Nb = \frac{\tau D_{B}\left(C_{w}-C_{\infty}\right)}{\left(\mu C_{p}\right)_{f}},\ Nt = \frac{\tau D_{T}\left(T_{w}-T_{\infty}\right)}{T_{\infty}\left(\mu C_{p}\right)_{f}}, \end{aligned}\right\} \tag{15}$$

After non-dimensionalization, the coefficient of skin-friction, local Nusselt, and Sherwood numbers are provided for engineering concern

$$\left.\begin{aligned} Cf_x &= 2\sqrt{\frac{n+1}{2}}.\frac{1}{\sqrt{\mathrm{Re}_x}}.\ f''(0),\quad Cf_y = 2\sqrt{\frac{n+1}{2}}.\frac{1}{\sqrt{\mathrm{Re}_y}}.\ g''(0) \\ Nu &= -\sqrt{\frac{n+1}{2}}.\sqrt{\mathrm{Re}_x}\,.\,\theta'(0),\quad Sh = -\sqrt{\frac{n+1}{2}}.\sqrt{\mathrm{Re}_x}\,.\,\phi'(0) \end{aligned}\right\} \tag{16}$$

Where $\mathrm{Re}_x = \dfrac{u_x(x)(x+y+z)}{\nu}$ & $\mathrm{Re}_y = \dfrac{v_x(x)(x+y+z)}{\nu}$ are local Reynolds numbers.

3. Solution Method by Finite Element Method:

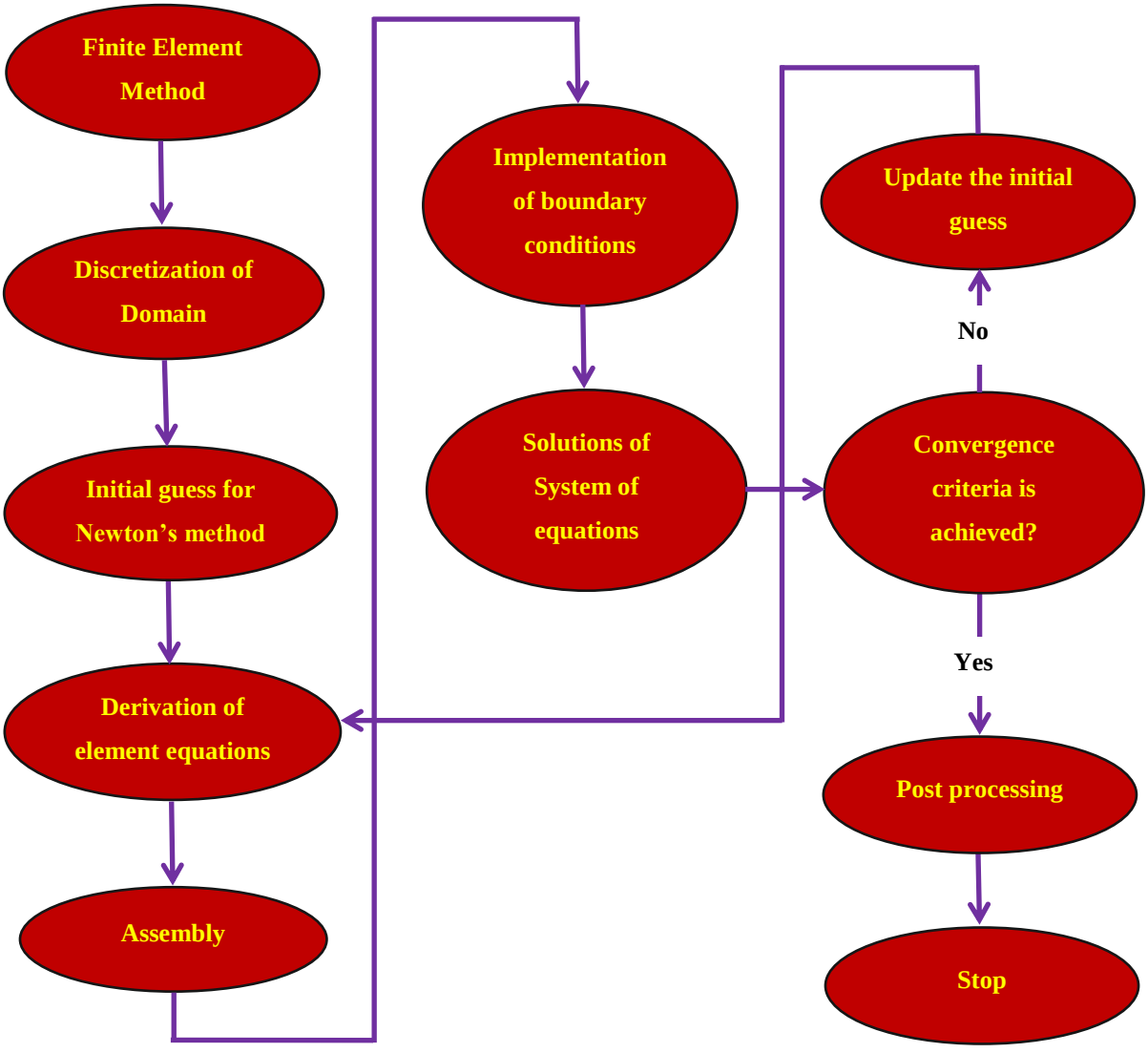

Fig. 2. Finite Element Method flow chart

Using the finite element technique to solve ordinary derivable equations and partial derivable equations is a highly efficient way of solving differential equations. As previously stated, the finite element technique is predicated on the notion of subdividing the domain into smaller pieces with finite dimensions, which are referred to as finite elements in this context. This is the most adaptable numerical approach known for engineering analysis at the time of this writing. It has been used to a broad variety of phenomena, including heat transport, Chemical reactions, electrical systems, acoustics, solid mechanics, and rigid body dynamics, and fluid dynamics to name a few examples. As seen in Fig. 2, utilising the finite element approach. In order to do these are the steps involved in finite element analysis must be completed:

- **Domain discretization into constituent parts:** Using the whole a limited number of subintervals are created from the interval using the finite element discretization, with each of these being referred to as an element.
- **Domain decomposition into elements:** The finite-element mesh is made up of all of the elements that were previously mentioned.
- To generate element equations, the following technique should be followed:
  a) Initial variations are made over the typical constituent of the mathematical model. (a single element from the mesh).
  b) When the variational problem has an approximate solution, by substituting the estimated solution the element equations are constructed into the previously established system, which is then solved for the variable.
  c) This matrix is formed by interpolating polynomials and is referred to as stiffness matrix.
- **Putting together and solving equations:** It is necessary to build all algebraic by requiring inter-element continuity in equations requirements on the elements of each equation. It is possible to develop by combining a higher number of algebraic equations, the entire domain is created.by a global finite-element model of
- **Implementation of limit conditions:** It is necessary to impose the equations' boundary conditions for the flow model that have been constructed.

There are a variety of numerical approaches that may used to resolve built-in equations, including the Gauss elimination approach, the Factorisation LU method, and others, to solve the created equations. It is vital to remember the form functions that are used to approximate real functions while working with real numbers. The whole a flow domain is separated into 10,000 sub-domainssimilar-sized quadratic components, with each component consisting of three nodes, for a total of 20,001 nodes in the domain. The 10,000 separate flow domains are used.similar-sized quadratic components. Following the creation of element equations, we

obtained a total of 80,004 non-linear equations for analysis. Following the application With a precision of 0.00001, Gauss elimination method is used to solve the remaining system of nonlinear equations using a numerical method. The integrations are solved with the help of the Gaussian quadrature that has been applied. The method's computer software was written in the MATHEMATICA programming language and ran on a desktop computer.

4. Program Code Validation:

Table-1.: comparing current finite element technique findings to previously published Khan et al. [31] for $h_1 = h_2 = h_3 = M = Le = \lambda = 0$

Pr	Current Nusselt number results	Results of Nusselt number Khan et al. [31]
7.0	2.39552013258100236889742	2.404797
13.0	2.69820114752365487520586	2.705551
25.0	3.27952114397690296349476	3.287794
50.0	4.10085629627341379938934	4.115197
100.0	5.32967698333289743987693	5.336685

For program code validation, table-1 compares the current Nusselt number (heat transfer rate) results determined by finite element approach to those previously reported by Khan et al. [31] combining the shooting technique with the Runge-Kutta integration method of fourth-to-fifth order in the absence of thermal radiation ,magnetic field, and Prandtl number impacts on the absence of slip parameter Velocity slip, jump parameter of Temperature, Concentration, Wall thickness parameter and Magnetic field effects. This table reveals a sturdy association between the present findings and those obtained by Khan et al. [31], as previously settled results.

5. Results and Discussion

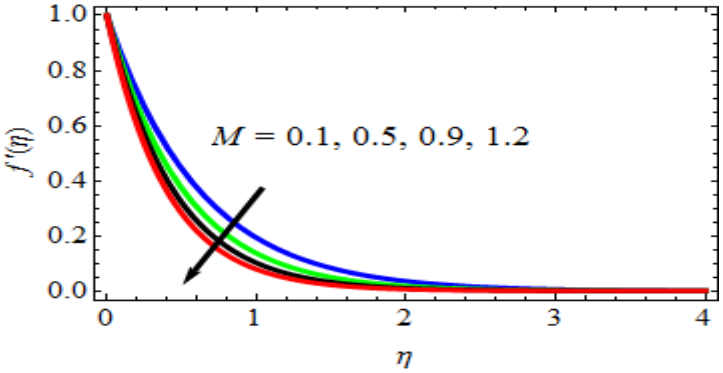

Fig. 3. Velocity profiles $f'(\eta)$ for variations of M

In this section, the general computations have been executed to investigate the impact of the various physical parameters namely *M* (Magnetic field Parameter), Pr (Prandtl number), *Nt* (Thermophoresis parameter), *Nb* (Brownian motion Parameter), *Le* (Lewis number), λ (Parameter of Wall thickness) and *n* (Velocity power index parameter) are presented through Figures 3, 4, 5, 6, 7, 8, 9, 10, 11, 12, 13, &14 for dimensionless profiles of velocity, concentration and temperature. Also, the same parameters effects are discussed on quantities of engineering namely Skin-friction coefficient, Nusselt number (heat transfer coefficient rate), Sherwood number (mass transfer coefficient rate) are discussed with help of numerical values in tabular forms. Figs. 3 and 4 design the velocity profiles $f'(\eta)$ and $g'(\eta)$ for different values of *M* (Magnetic field parameter). Observations show that fields of velocity $f'(\eta)$ and $g'(\eta)$ decline when the value of M increases. As a result of the fluid's tendency to flow more slowly when there is an applied magnetic field, the heftiness of the velocity and momentum boundary layers tends to decrease.. The influence of *n* (Velocity power index parameter) on profiles of velocity $f'(\eta)$ and $g'(\eta)$ are discussed in Figs. 5 and 6. From these two figures, Observations show that the profiles of velocity $f'(\eta)$ and $g'(\eta)$ are increasing as n increases in value (Velocity power index parameter).

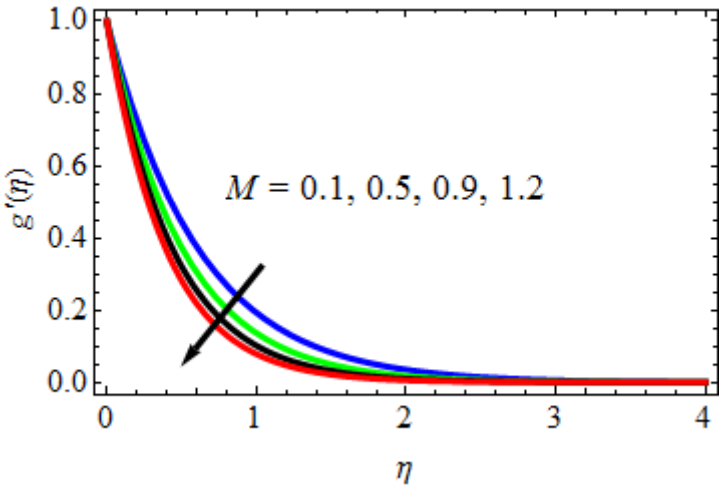

Fig. 4. Profiles of Velocity $g'(\eta)$ for variations of *M*

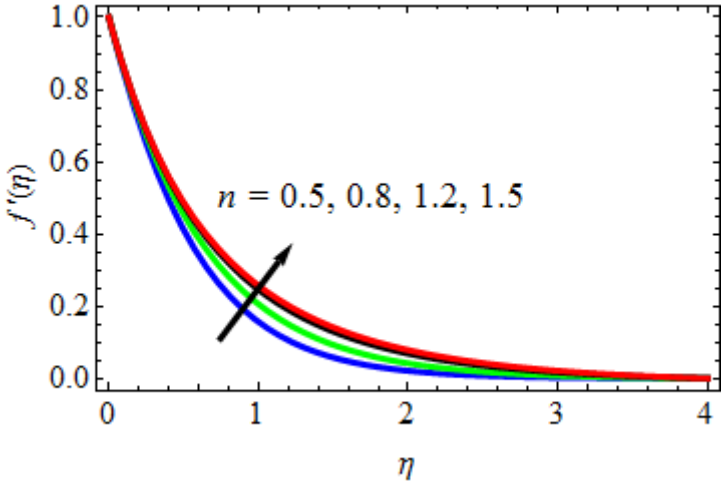

Fig. 5. Velocity Profiles $f'(\eta)$ for variations of *n*

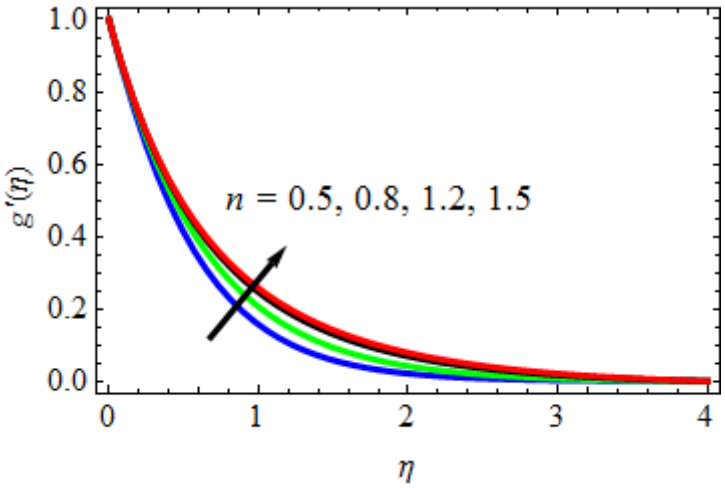

Fig. 6. Velocity Profiles $g'(\eta)$ for variations of *n*

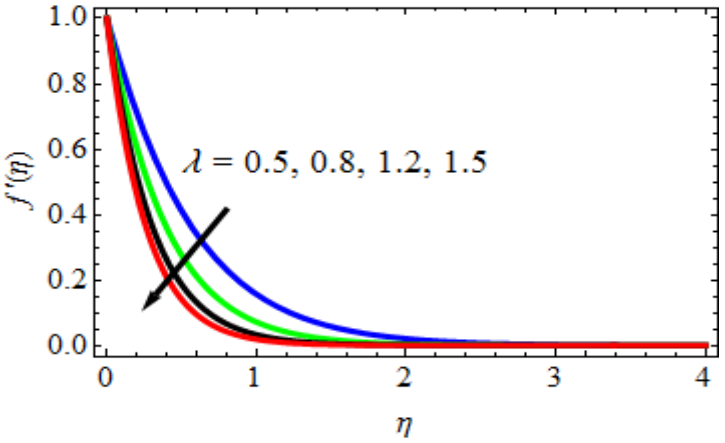

Fig. 7. Velocity Profiles $f'(\eta)$ for variations of λ

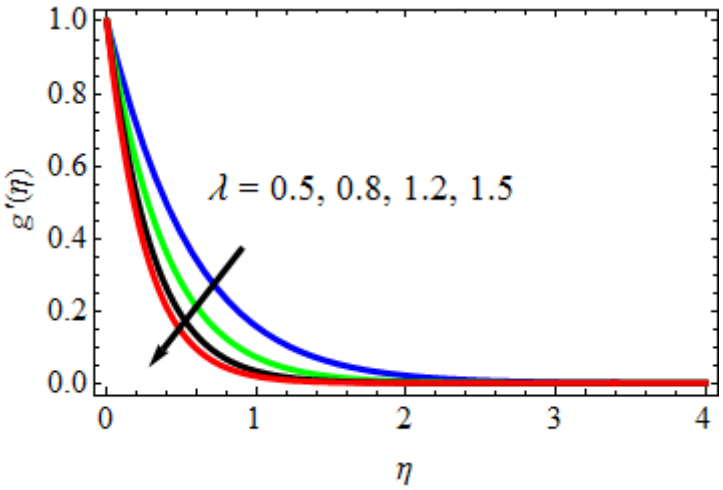

Fig. 8. Velocity Profiles $g'(\eta)$ for variations of λ

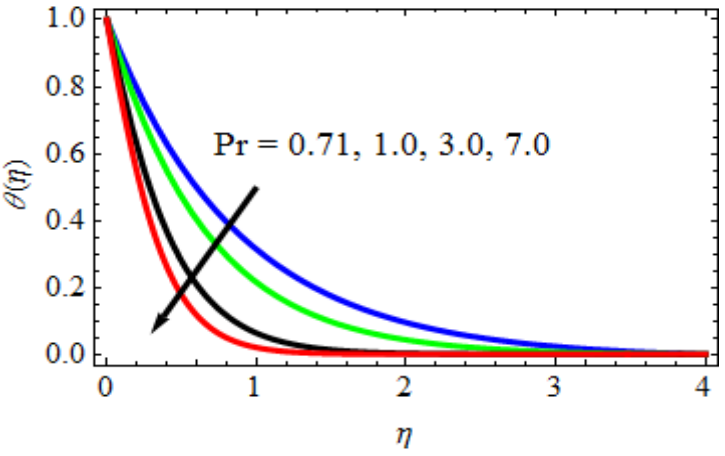

Fig. 9. Temperature profiles $\theta(\eta)$ for variations of Pr

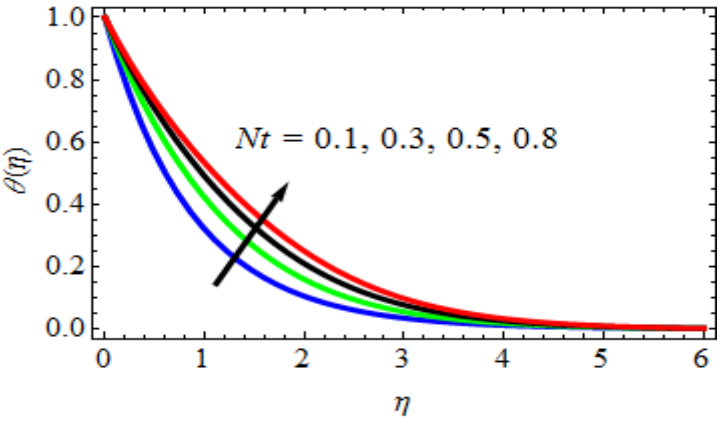

Fig. 10. Temperature profiles $\theta(\eta)$ for variations of *Nt*

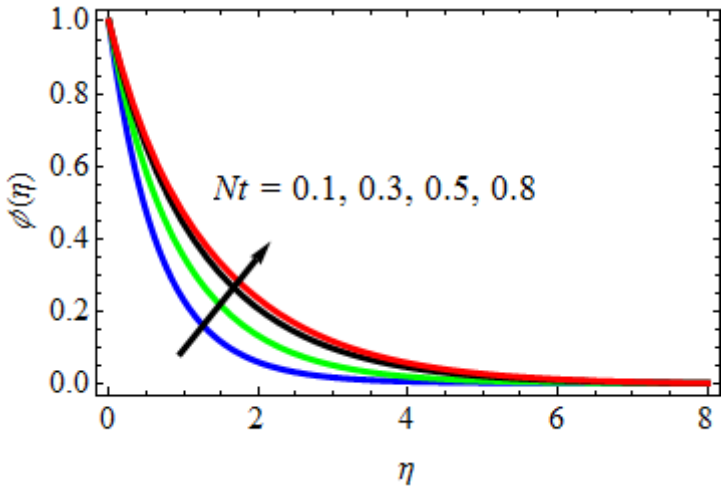

Fig. 11. Concentration profiles $\phi(\eta)$ for variations of *Nt*

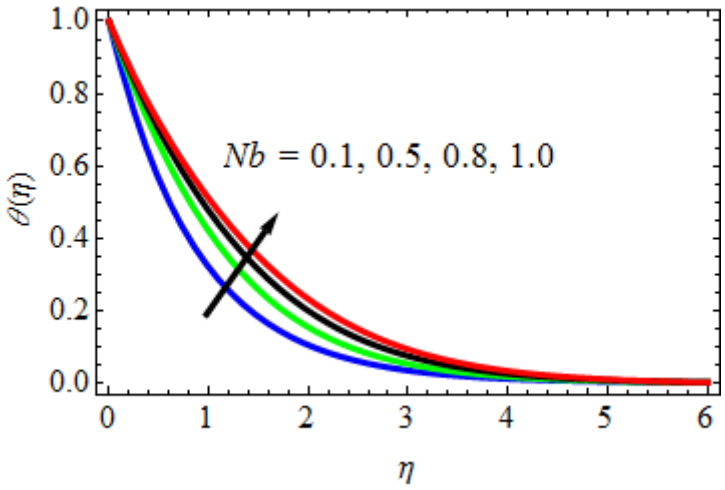

Fig. 12. Profiles of Temperature $\theta(\eta)$ for variations of *Nb*

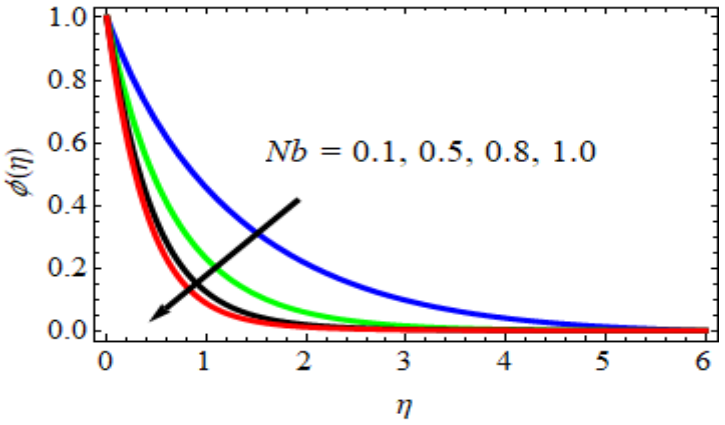

Fig. 13. Concentration profiles $\phi(\eta)$ for variations of *Nb*

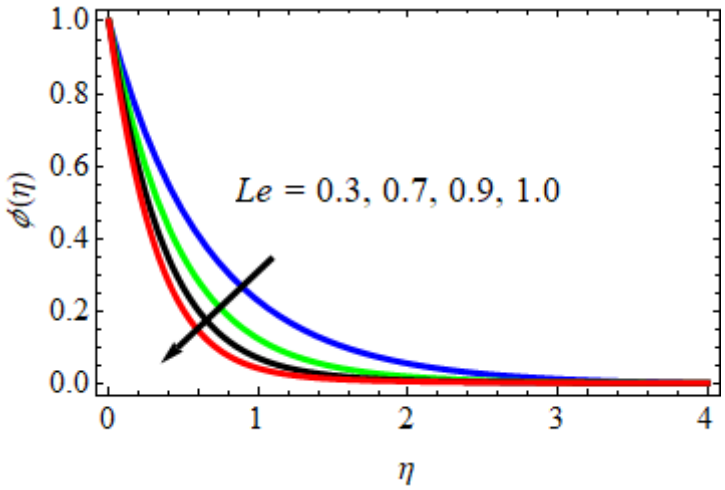

Fig. 14. Profiles of Concentration $\phi(\eta)$ for variations of *Le*

Table-2.: Numerical values of Skin-friction coefficient Cf_x for variations of *M*, Pr, *Nt*, *Nb*, *n*, λ and *Le*

M	Pr	*Nt*	*Nb*	*n*	λ	*Le*	Cf_x
0.1	0.71	0.1	0.1	0.5	0.5	0.3	1.758662015478899
0.5							1.694349691625319
0.9							1.676981348483593
	1.00						1.678787308591813
	7.00						1.659748399843473
		0.3					1.780374183498384
		0.5					1.804646034033647
			0.5				1.775691347863989
			0.8				1.790374298343794
				0.8			1.786587418734738
				1.2			1.804687519833439
					0.8		1.725696923983984
					1.2		1.703255479837383
						0.7	1.716743899389843
						0.9	1.698878789782878

From Figs. 7 and 8, the authors have discussed the velocity variations profiles $f'(\eta)$ and $g'(\eta)$ for different values of λ (Parameter of Wall thickness) through curves. The profiles of velocity $f'(\eta)$ and $g'(\eta)$ from these two pictures are in decreasing as the values of increase λ (parameter Wall thickness). Fig. 9 shows the impact of Pr (Prandtl number) on the temperature of fluid. The fluid's temperature gradient reduces as Pr's value rises. The momentum diffusivity rises and overtakes the thermal diffusivity as Pr rises. The fluid's velocity is high enough to aid in the fluid's ability to transfer heat. This accelerates the rate of heat dissipation and thins the boundary layer.. From Figs. 10 and 11, it is observed that with the rising values of *Nt* (Parameter of Thermophoresis)the temperature and concentration profiles are increases. Generally, Thermophoresis parameter aids in determining the thickness of temperature and concentration distributions' boundary layers.. As significance, raised the both profiles . Also, the authors have scrutinized from Figs. 12 and 13 that ascending in the *Nb* (Parameter of Brownian motion) lowers the concentration fields and raises the temperature. In actuality, not all nanoparticles have equivalent thermophoresis and Brownian motion coefficient values. This proves the physical scenery of *Nb*. Fig. 14 on the dimensionless concentration profiles depicts by the influence of the Lewis number (*Le*). The ratio of thermal and mass diffusivity is defined by the dimensionless Lewis number . The thermal boundary layer thickness is increased by increasing the value of *Le*, whereas, the boundary layer thickness is decreased due to the nanoparticle volume concentration.. The effects of engineering parameters such as *M* (Parameter Magnetic field), Pr (Prandtl number), *Nt* (Parameter of Thermophoresis), *Nb* (Parameter of Brownian motion), *Le* (Lewis number), λ (Wall thickness parameter) and *n* (Velocity power index parameter) on Skin-friction coefficient Cf_x is discussed in table-2. From this table, it is observed that with increasing values of *Nt* (Thermophoresis parameter)the skin-friction coefficient Cf_x is increases, *Nb* (Brownian motion parameter), *n* (Parameter of Velocity power index) and Cf_x decreasing with increasing values of *M* (Parameter of Magnetic field), Pr (Prandtl number), *Le* (Lewis number) and λ (Wall thickness parameter). The effects of engineering parameters such as *M* (Magnetic field parameter), Pr (Prandtl number), *Nt* (Parameter Thermophoresis), *Nb* (Brownian motion parameter), *Le* (Lewis number), λ (Wall thickness parameter) and *n* (Velocity power index parameter) on Skin-friction coefficient Cf_y is discussed in table-3. From this table, it shows that the skin-friction coefficient Cf_y is growing with rising values of *Nt* (Thermophoresis parameter), *Nb* (Parameter of Brownian motion), *n* (Velocity power index parameter) and Cf_y declining with growing values of *M* (Parameter Magnetic field), Pr (Prandtl number), *Le* (Lewis number) and λ (Wall thickness parameter).

Table-3.: Skin-friction coefficient Cf_y **n**umerical values of for variations of *M*, Pr, *Nt*, *Nb*, *n*, λ and *Le*

M	Pr	*Nt*	*Nb*	*n*	λ	*Le*	Cf_y
0.1	0.71	0.1	0.1	0.5	0.5	0.3	0.586794720895124
0.5							0.557412585156631
0.9							0.529987418529654
	1.00						0.537884107679873
	7.00						0.506758234798312
		0.3					0.626789983170608
		0.5					0.647857987289283
			0.5				0.612342938057985
			0.8				0.637898524674592
				0.8			0.614475939874437
				1.2			0.638938734982384
					0.8		0.567898718457846
					1.2		0.540930347817758
						0.7	0.550948573187302
						0.9	0.538787654048956

Table-4.: For different values of Pr, *Nb* and *Nt*, rate of heat transfer coefficient *Nu* values

Pr	*Nb*	*Nt*	*Nu*
0.71	0.1	0.1	0.478889398493848
1.00			0.435906262737472
3.00			0.408980795827139
	0.5		0.519841564239839
	0.8		0.535987064317699
		0.3	0.500934798738931
		0.5	0.529843891964392

Table 4 shows the numerical rates of heat transfer coefficient in terms of the Nusselt number for various values of Pr (Prandtl number), *Nt* (Parameter of Thermophoresis), *Nb* (Parameter of Brownian

motion). Increasing values of Nt (the thermophoresis parameter) and Nb (the Brownian motion parameter) cause the rate of heat transfer coefficient to progressively increase, but increasing values of Prandtl number (Pr) have the opposite effect. Table 5 shows the numerical rates of mass transfer coefficient in terms of Sherwood numbers for various values of Le (Lewis number), Nt (thermophoresis parameter), and Nb (Brownian motion parameter). Increasing values of Nt (the thermophoresis parameter) and Nb (the Brownian motion parameter) cause the rate of mass transfer coefficient to progressively increase, but increasing values of Lewis number (Le) have the opposite effect.

Table-5.: Values for different values of *Le*, *Nb* and *Nt* ,rate of mass transfer coefficient *Sh*

Le	*Nb*	*Nt*	*Sh*
0.71	0.5		0.308798465818468
1.00			0.257698731984770
3.00			0.236793873948793
	0.5		0.266981398739209
	0.8		0.240983647637426
		0.3	0.336793418798748
		0.5	0.350987398743366

6. Conclusions:

In this current research work, RK method implements measures to provide the nanofluid parameters numerical solutions in three dimensional flow. In order to evaluate the impact of well-known fluid characteristics on the flow of nanofluid through three-dimensional structures, numerical solutions are utilised. The results are:

a) Superior values of M and λ falls down the profiles of velocity $f'(\eta)$ and $g'(\eta)$.

b) Increase in values of $f'(\eta)$ and $g'(\eta)$ has been observed for better values of n.

c) Temperature $\theta(\eta)$ profiles minimizes by advanced Prandtl number. On the other hand, opposite trend is observed for domineering fluid parameter rs *Nb* and *Nt*.

d) Profiles of Concentration $\phi(\eta)$ extended for *Nt* and reduces for *Nb* and *Le*.

e) Finally, comparison of present research work with Khan et al. [31] is considered for limited values of these parameters.

References:

1. Z. Uddin, M. Kumar, Hall and ion-slip effect on MHD boundary layer flow of a micro polar fluid past a wedge, Sci Iran B, 20 (3) (2013), pp. 467-476, 10.1016/j.scient.2013.02.013.
2. W. N. Mutuku-Njane, O. D. Makinde, On hydromagnetic boundary layer flow of nanofluids over a permeable moving surface with newtonian heating, Latin Am Appl Res, 44 (2014), pp. 57-62.
3. G. M. Ablel-Rahman, Thermal diffusion and MHD effects on combined free forced convection and mass transfer flow of a viscous fluid flow through a porous medium with heat generation, Chem Eng Technol, 31 (2008), pp. 554-559, 10.1002/ceat.200700487.
4. M. A. Seddeek, M. S. Abdelmeguid, Hall and Ion-slip effects on magneto-micropolar fluid with combined forced and free convection in boundary layer flow over a horizontal plate, J. KSAIM, 8 (2) (2004), pp. 51-73.
5. S. Ahmed, A. Batin, Magnetohydrodynamic heat and mass transfer flow with induced magnetic field and viscous dissipative effects, Latin Am Appl Res, 44 (2014), pp. 9-17.
6. P. C. Ram, The effects of hall and ion slip currents on free convective heat generating flow in a rotating fluid, Int J Energy Res, 19 (5) (1995), pp. 371-376, 10.1002/er.4440190502.
7. B. K. Jha, C. A. Apere, Combined effect of Hall and ion-slip currents on unsteady MHD Couette flows in a rotating system, J Phys Soc Jpn, 79 (10) (2010), Article 104401, 10.1143/JPSJ.79.104401.
8. D. Sarma, N. Ahmed, H. Deka, MHD free convection and mass transfer flow past an accelerated vertical plate with chemical reaction in presence of radiation, Latin Am Appl Res, 44 (2014), pp. 1-8.
9. H. F. Oztop, E. Abu-Nada, Numerical study of natural convection in partially heated rectangular enclosures filled with nanofluids, Int J Heat Mass Transf, 29 (2008), pp. 1326-1336.
10. N. A. Reddy, M. C. Raju, S. V. K. Varma, Thermo diffusion and chemical effects with simultaneous thermal and mass diffusion in MHD mixed convection flow with Ohmic heating, J Naval Architect Mar Eng, 6 (2009), pp. 84-93.
11. M. A. Seddeek, The effects of hall and ion-slip cur-rents on magneto-micropolar fluid and heat transfer over a non-isothermal stretching sheet with suction and blowing, Proc R Soc Lond A, 457 (2001), pp. 3039-3050, 10.1098/rspa.2001.0847.
12. I. A. Sara, M. M. Bhatti, The study of non-Newtonian nanofluid with Hall and ion slip effects on peristaltically induced motion in a non-uniform channel, RSC Adv, 8 (2018), pp. 7904-7915, 10.1039/c7ra13188g.

13. Jitendra Kumar Singh, C. T. Srinivasa, Unsteady natural convection flow of a rotating fluid past an exponential accelerated vertical plate with Hall current, ion-slip and magnetic effect, Multidiscip Model Mater Struct, 14 (2) (2018), pp. 216-235, 10.1108/MMMS-06-2017-0045
14. G. Ibanez, Entropy generation in MHD porous channel with hydrodynamic slip and convective boundary conditions, *Int. J. Heat Mass Transf*., 80 (2015), pp. 274-280.
15. A. Aziz, A similarity solution for laminar thermal boundary layer over a flat plate with a convective surface boundary condition, *Commun. Nonlinear Sci. Numer. Simul.*, 14 (2009), pp. 1064-1068.
16. J. A. Khan, M. Mustafa, T. Hayat, A. Alsaedi, Three-dimensional flow of nanofluid over a nonlinearly stretching sheet: an application to solar energy, Int. J. Heat Mass Trans., 86 (2015), pp. 158-164.
17. T. Hayat, M. Imtiaz, A. Alsaedi, Unsteady flow of nanofluid with double stratification and magnetohydrodynamics, Int. J. Heat Mass Trans., 92 (2016), pp. 100-109.
18. M. Ferdows, M. Shamshuddin, S. O. Salawu, Numerical simulation for the steady nanofluid boundary layer flow over a moving plate with suction and heat generation, SN J. Appl. Sci., 3 (2021), p. 264.
19. T. Sravan Kumar, P.A. Dinesh, O. D. Makinde, Impact of Lorentz force and viscous dissipation on unsteady nanofluid convection flow over an exponentially moving vertical plate, Math. Model Comput. Simul., 12 (2020), pp. 631-646.
20. P. Yogeswara Reddy, G. S. S. Raju, Influence of magnetic field and radiation on heat and mass transfer flow of nano fluid over an inclined vertical plate embedded in porous medium Turkish J. Comput. Math. Educ., 12 (10) (2021), pp. 4412-4426
21. S. Hussain, Finite element solution for MHD flow of nanofluids with heat and mass transfer through a porous media with thermal radiation, viscous dissipation and chemical reaction effects, Adv. Appl. Math. Mech., 9 (2017), pp. 904-923.
22. S. P. Anjali Devi, P. Suriyakumar, Effect of magnetic field on Blasius and Sakiadis flow of nanofluids past an inclined plate, J. Taibah Univ. Sci., 11 (6) (2017), pp. 1275-1288.
23. Yanhai Lin, LiancunZheng, Xinxin Zhang, Lianxi Ma and Goong Chen, MHD pseudo-plastic nanofluid unsteady flow and heat transfer in a finite thin film over stretching surface with internal heat generation, Int. J. Heat Mass Transf., Vol. 84, pp. 903-911, 2015.
24. M. Farooq, M. Ijaz Khan, M. Waqas, T. Hayat, A. Alsaedi and M. Imran Khan, MHD stagnation point flow of viscoelastic nanofluid with non-linear radiation effects, J. Mol. Liquids, Vol. 221, pp. 1097-1103, 2016.

25. T. Hayat, G. Bashir, M. Waqas and A. Alsaedi, MHD 2D flow of Williamson nanofluid over a nonlinear variable thicked surface with melting heat transfer, J. Mol. Liquids, Vol. 223, pp. 836-844, 2016.
26. S. Nadeem, R. Mehmood, N. S. Akbar, Partial slip effect on non-aligned stagnation point nanofluid over a stretching convective surface, *Chin. Phys. B*, 24 (1) (2015), pp. 1-8.
27. T. Hayat, A. Aziz, T. Muhammad, B. Ahmad, Influence of magnetic field in three-dimensional flow of couple stress nanofluid over a nonlinearly stretching surface with convective condition, *PLOS ONE*, 10 (12) (2015), p. e0145332.
28. A. López, G. Ibáñez, J. Pantoja, J. Moreira, O. Lastres, Entropy generation analysis of MHD nanofluid flow in a porous vertical microchannel with nonlinear thermal radiation, slip flow and convective-radiative boundary conditions, Int. J. Heat Mass Transf., 107 (2017), pp. 982-994.
29. Vemula Rajesh, Mikhail A. Sheremet, Hakan F. Öztop, Impact of hybrid nanofluids on MHD flow and heat transfer near a vertical plate with ramped wall temperature, Case Stud. Therm. Eng., 28 (2021), p. 101557.
30. M. Siavashi, H. R. Talesh Bahrami, E. Aminian, H. Saffari, Numerical analysis on forced convection enhancement in an annulus using porous ribs and nanoparticle addition to base fluid, J. Cent. South Univ., 26 (5) (2019), pp. 1089-1098, 10.1007/s11771-019-4073-z.
31. J. A. Khan, M. Mustafa, T. Hayat, M. Asif Farooq, A. Alsaedi, S. J. Liao, On model for three-dimensional flow of nanofluid: An application to solar energy, Journal of Molecular Liquids, Vol. 194, 2014, pp. 41-47.